OPEN

NPG Asia Materials (2016) 8, e325; doi:10.1038/am.2016.166
www.nature.com/am

ORIGINAL ARTICLE

Observation of quasi-two-dimensional Dirac fermions in $ZrTe_5$

Xiang Yuan[1,2,5], Cheng Zhang[1,2,5], Yanwen Liu[1,2], Awadhesh Narayan[3,4], Chaoyu Song[1,2], Shoudong Shen[1,2], Xing Sui[1,2], Jie Xu[1,2], Haochi Yu[1,2], Zhenghua An[1,2], Jun Zhao[1,2], Stefano Sanvito[3], Hugen Yan[1,2] and Faxian Xiu[1,2]

Since the discovery of graphene, layered materials have attracted extensive interest owing to their unique electronic and optical characteristics. Among them, Dirac semimetals, one of the most appealing categories, have been a long-sought objective in layered systems beyond graphene. Recently, layered pentatelluride $ZrTe_5$ was found to host signatures of a Dirac semimetal. However, the low Fermi level in $ZrTe_5$ strongly hinders a comprehensive understanding of the whole picture of electronic states through photoemission measurements, especially in the conduction band. Here, we report the observation of Dirac fermions in $ZrTe_5$ through magneto-optics and magneto-transport. By applying a magnetic field, we observe a $\sqrt{B}$ dependence of the inter-Landau-level resonance and Shubnikov–de Haas (SdH) oscillations with a nontrivial Berry phase, both of which are hallmarks of Dirac fermions. The angle-dependent SdH oscillations show a clear quasi-two-dimensional feature with a highly anisotropic Fermi surface and band topology, in stark contrast to the three-dimensional (3D) Dirac semimetal such as Cd_3As_2. This is further confirmed by the angle-dependent Berry phase measurements and the observation of bulk quantum Hall effect (QHE) plateaus. The unique band dispersion is theoretically understood: the system is at the critical point between a 3D Dirac semimetal and a topological insulator phase. With the confined interlayer dispersion and reducible dimensionality, our work establishes $ZrTe_5$ as an ideal platform for exploring the exotic physical phenomena of Dirac fermions.
NPG Asia Materials (2016) **8,** e325; doi:10.1038/am.2016.166; published online 11 November 2016

INTRODUCTION

Layered materials, formed by stacking strongly bonded layers with weak interlayer coupling,[1–10] have drawn immense attention in fundamental studies and device applications owing to their tunability in band structures and Fermi energy.[3,4,11–13] Unlike other layered materials such as MoS_2 and BN, graphene stands out as an appealing candidate, as it is featured with a linear energy dispersion and low-energy relativistic quasi-particles.[9,14,15] Many exotic phenomena, such as a half-integer quantum Hall effect (QHE)[1,2] and Klein tunneling,[16] have been realized in graphene. Along this line, extensive efforts were also devoted to exploring new Dirac semimetal states in other layered systems beyond graphene.[5,6]

Pentatelluride $ZrTe_5$ with a layered orthorhombic structure has been widely studied since the 1980s for its resistivity anomaly[17–19] and large thermopower.[20,21] For a long time, $ZrTe_5$ was considered to be a semimetal or degenerated semiconductor with a parabolic energy dispersion.[10,22] However, a recent study[7] revealed a linear dispersion in $ZrTe_5$ bulk states along with a chiral magnetic effect, hosting the signatures of a Dirac semimetal. Nevertheless, owing to the relatively low Femi level in $ZrTe_5$, a complete understanding of the band structure, especially the conduction band, remains elusive from angle-resolved photoemission spectroscopy (ARPES) measurements, making it challenging to confirm the existence of Dirac fermions. Meanwhile, the layered structure of $ZrTe_5$ gives rise to a weak interlayer coupling that should release the confinement on the interlayer dispersion of Dirac fermions as in the case of cuprates.[23] The interplay between Dirac fermions and the interlayer confinement may result in intriguing physical properties yet to be explored.

Here, we report the observation of massless Dirac fermions in layered $ZrTe_5$ based on two independent experiments: magneto-optics and magneto-transport. An external magnetic field leads to the Landau quantization of Bloch electrons, enabling us to probe the band structure and carrier dynamics in $ZrTe_5$. A $\sqrt{B}$ dependence of inter-Landau-level resonance is observed, indicating a linear band dispersion. Owing to the high electron mobility and low Fermi level, we are able to detect the Shubnikov–de Haas (SdH) oscillations close to the quantum limit, from which a non-trivial Berry phase is obtained. Both of them are well-established signatures for

[1]State Key Laboratory of Surface Physics and Department of Physics, Fudan University, Shanghai, China; [2]Collaborative Innovation Center of Advanced Microstructures, Nanjing University, Nanjing, China; [3]School of Physics, AMBER and CRANN Institute, Trinity College, Dublin, Ireland and [4]Department of Physics, University of Illinois at Urbana–Champaign, Urbana, IL, USA
[5]These authors contributed equally to this work.
Correspondence: Professor F Xiu or Professor H Yan, State Key Laboratory of Surface Physics and Department of Physics, Fudan University, Room 406, Advanced Materials Building, 2205, Songhu Road, Shanghai 200433, China.
E-mail: Faxian@fudan.edu.cn or Hgyan@fudan.edu.cn
Received 11 February 2016; revised 17 August 2016; accepted 26 August 2016

ultra-relativistic quasi-particles in crystals. Furthermore, the angle-dependent magneto-transport reveals a quasi-two-dimensional (2D) Fermi surface. A striking anisotropy is witnessed in the band dispersion characteristics along different crystal orientations, and along the b-axis (the layer-stacking direction), a carrier mass heavier than that of the free electron suggests a nonlinear dispersion. This conclusion is further supported by the critical evidence of the trivial Berry phase and the observed bulk QHE. $ZrTe_5$ is theoretically analyzed to be at a critical phase between a three-dimensional (3D) Dirac semimetal and a weak topological insulator. Reducible dimensions in $ZrTe_5$ (2D and 1D) attained upon exfoliation also promises possible device applications.

MATERIALS AND METHODS

Single-crystal synthesis

High-quality $ZrTe_5$ single crystals were synthesized via the iodine vapor transport method in a two-zone tube furnace. Stoichiometric amounts of high-purity Zr and Te elements were placed in a quartz tube and sealed under vacuum. $ZrTe_5$ is crystallized during a chemical transport reaction process (14 days) with a temperature gradient from 500 to 450 °C. We use a transport agent of iodine with a concentration of 10 mg cm^{-3}. The growth rate along the a-axis is much faster than those of b-axis and c-axis, yielding needle-like samples. The chemical ratio is found to be 1 : 5 for Zr/Te, determined by energy dispersive X-ray analysis in scanning electron microscopy.

Magneto-optics measurements

$ZrTe_5$ was freshly cleaved and subjected to an applied magnetic field parallel to the stacking axis (Faraday geometry) at liquid helium temperature. An infrared light from a broadband light source is modulated by an interferometer and vibration mirrors in the Fourier transform infrared spectrometer. The light was guided through a light pipe and focused on the sample with a millimeter spot by a parabolic cone (Supplementary Figure S1). A bolometer was used to measure the intensity of reflection light simultaneously with Fourier transform infrared spectrometer.

Magneto-transport measurements

Freshly cleaved $ZrTe_5$ was measured using a standard six-terminal Hall bar geometry in a physical property measurement system. Stanford Research (Sunnyvale, CA, USA) 830 Lock-in amplifiers were used to measure the electrical signals with a magnetic field up to 9 T that applied for various orientations of the applied magnetic field.

Sample exfoliation

$ZrTe_5$ was first exfoliated on Scotch tape and then transferred onto a 300 nm/300 μm SiO_2/Si substrate. The flakes with different thicknesses can be identified by different colors. To enhance the productivity of the 1D structure and avoid contamination, polydimethylsiloxane was used to transfer the exfoliated samples.

RESULTS

Under an external magnetic field B, the charged particles can occupy discrete orbits and form Landau levels. In a classical system described by the Schrodinger equation, by ignoring the dispersion along the parallel direction, the energy of each Landau level can be strictly derived as $E_n = (n+1/2)\hbar\omega_c$, $n = 0,1,2...$ where $\omega_c = eB/m^*$, n, $\hbar$ and e denote the cyclotron angular frequency, the Landau-level index, the reduced Plank's constant and the elementary charge, respectively.

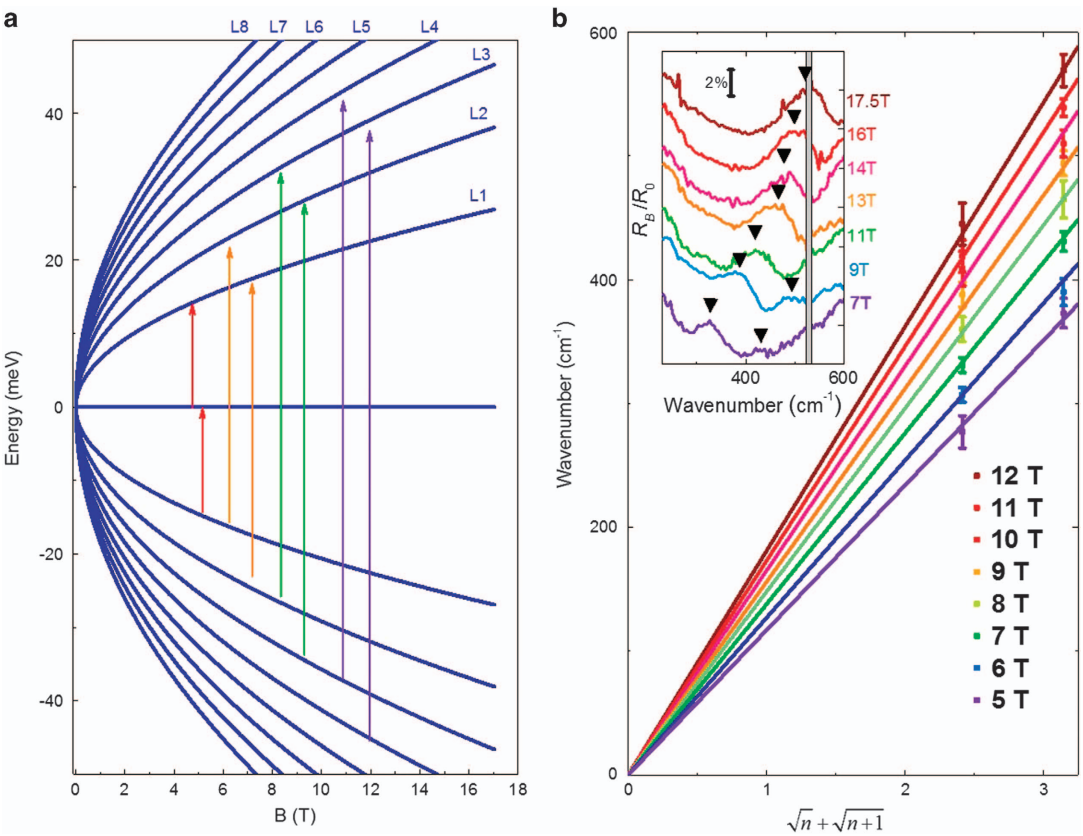

Figure 1 Landau-level fan chart and normalized magnetoreflection of $ZrTe_5$. (**a**) Landau levels in $ZrTe_5$ as a function of magnetic field. Arrows show the allowable optical transitions. Different colors denote different resonance energies. (**b**) The resonance energy versus $\sqrt{n}+\sqrt{n+1}$ under different magnetic fields. The straight line is for eye-guide. The inset shows normalized reflection spectra under different magnetic fields. Triangles denote the peak positions.

As E_n increases linearly with B, magneto-optics measurements are usually applied to obtain the effective mass m^* of these classical quasi-particles. However, in Dirac materials, where the electrons are described by the Dirac equation, when ignoring the parallel dispersion, the energy of the relativistic quasi-particles can be derived as

$$E_n = \mathrm{sgn}(n)\sqrt{2v_F{}^2 eB\hbar|n|}, n = \pm 0, 1, 2... \quad (1)$$

Here E_n follows a square root relation with the magnetic field as depicted in Figure 1a. The Fermi velocity determines the evolution of the Landau-level energy in Dirac systems with a magnetic field. The assumption of $k_z = 0$ is valid for magnetic fields applied along the b-axis direction. Although the Landau levels have a finite dispersion in the k_z direction, magneto-optical reflection occurs at $k_z = 0$ where the joint density of states of the Landau levels corresponding to the transition are optimal.[24]

Landau-level transitions give resonance peaks in the reflection spectra. To confirm the validity of Equation (1) in $ZrTe_5$, we measured the reflection spectra of bulk $ZrTe_5$ crystals under various magnetic fields at liquid helium temperature. The single crystal of $ZrTe_5$ used in this study was grown by the iodine vapor transport method that is different from the flux method.[7,25,26] The as-grown crystals crystallized in the orthorhombic layered structure with space group D_{2h}^{17}.[17] The prismatic chains of $ZrTe_3$ run along the a-axis and are linked by the zigzag chains of Te along the c-axis. These 2D layers then stack along the b-axis, forming the bulk crystal. To avoid oxidation and contamination, the samples were freshly cleaved before experiments. During the magneto-infrared measurements, the magnetic field is parallel to the b-axis (stacking axis) of the samples. The measured reflection spectra are normalized by the spectrum at zero magnetic field. The detailed experimental setup for the magneto-infrared measurements is provided in Supplementary Figure S1. Several reflection peaks can be well resolved in the normalized reflection spectra measured under different magnetic fields (Figure 1b, inset). The blocked gray area originates from 60 Hz harmonics. As these reflection maxima systematically shift toward higher energy with the increasing magnetic field, we conclude that the resonance is coming from the inter-Landau-level transitions, as determined by electric-dipole-selection rules.[27] The incident photons excite the electrons from the occupied valance band to the unoccupied conduction band (Figure 1a) following $\Delta n = n \pm 1$. Thus, the resonance energy of inter-Landau-level transitions is given by

$$E_{\mathrm{resonance}} = E_n + E_{n+1} = 2v_F\sqrt{eB\hbar}(\sqrt{n} + \sqrt{n+1}), n = 0, 1, 2... \quad (2)$$

The energy ratio between the second (right) and the first (left) resonance peak (Figure 1b, inset) is 1.3, almost the same value as $(\sqrt{2} + \sqrt{3}) : (\sqrt{1} + \sqrt{2})$. Thus, the first peak is assigned to be the transition from L_{-1} to L_2 or from L_{-2} to L_1 (orange arrows in Figure 1a), where L_n represents the nth Landau level. Peaks at higher energy should correspond to the higher Landau-level index. Keeping this in mind, we plot the peak positions with $\sqrt{n} + \sqrt{n+1}$. As shown in Figure 1b, for different magnetic fields, the data points are well aligned on a straight line with the y-axis offset close to zero, proving the validity of Equations (1) and (2) and the Landau index assignment. These phenomena show a striking difference from classical systems such as narrow bandgap semiconductors (as well as trivial bulk state of topological insulators) in which Landau levels are equally spaced and the resonance energy is proportional to B. The assignment of the Landau index quantitatively leads to a Fermi velocity of $v_F = 2 \times 10^5\ \mathrm{m\ s^{-1}}$ that corresponds to the average slope of the band dispersion in the $k_a - k_c$ plane.

Another key feature of massless Dirac fermions in magneto-infrared spectra,[15,27,28] as expressed by Equation (1), is the $\sqrt{B}$ dependence of the transition energy for a fixed Landau index. To analyze the evolution of the peak position with the magnetic field (Figure 2, inset), we plotted the peak position of the normalized reflection spectrum against $\sqrt{B}$ (Figure 2). It is evident that the peak position of one Landau-level transition under different fields forms a straight line, indicating a $\sqrt{B}$ dependence of resonance energy that is different from the B dependence of a classical system. The straight lines in Figure 2 are the linear fit to the peak positions that point to the origin of the coordinates, consistent with Equation (2). We noticed a recent report with a similar field dependence for the resonance energy, but with a different Landau-level index and Fermi level.[26] The slopes of the lines derive the same value of the Fermi velocity as determined in Figure 1b. The Landau index can also be obtained by comparing the slopes of different sets of transitions. The most prominent peaks in the Figure 1b inset are determined to be L_{-2} to L_1 (L_{-1} to L_2). We note that the transition for the lower indices (L_0 to L_1) is not observable because of the strong phonon absorption of $ZrTe_5$ when the excitation energy is $< 200\ \mathrm{cm^{-1}}$ (Supplementary Figure S2). No clear sign of a quasi-particle gap was observed in the experimental limit (refer to section XII in the Supplementary Information). Both $\sqrt{n}$ and $\sqrt{B}$ dependence in the magneto-infrared study provides a consolidate evidence for the existence of Dirac fermions in $ZrTe_5$.

Recently, 3D Dirac semimetals have been extensively studied.[29,30] The definition of the 3D Dirac semimetal requires a linear dispersion along all directions, including the high symmetry axes in crystals.[30] To confirm the dimensionality of the observed Dirac state, it is definitely insufficient to solely examine the energy dispersion in the a–c plane by the cyclotron resonance through SdH oscillations/magneto-optic or by ARPES spectroscopy. In contrast, direct evidence for the linear dispersion along the b-axis, such as linear $E - k_b$ from ARPES, $\sqrt{B}$ cyclotron energy from magneto-optical spectroscopy (a, b and b, c planes) or the extraction of a Berry phase of π from low-temperature transport measurements (a, b and b, c planes), is required to claim the 3D feature of the massless Dirac fermions.

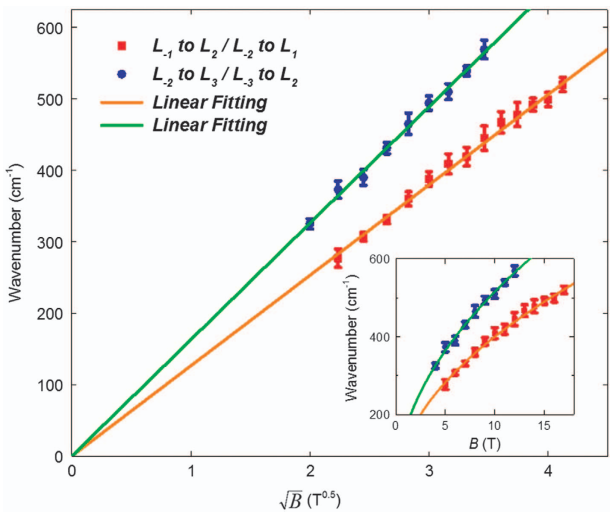

Figure 2 Magnetoreflectivity in $ZrTe_5$. Reflectivity maxima frequencies plotted with $\sqrt{B}$. The observed inter-Landau-level resonance clearly follows a $\sqrt{B}$ dependence. The inset shows the reflectivity maxima frequency versus B.

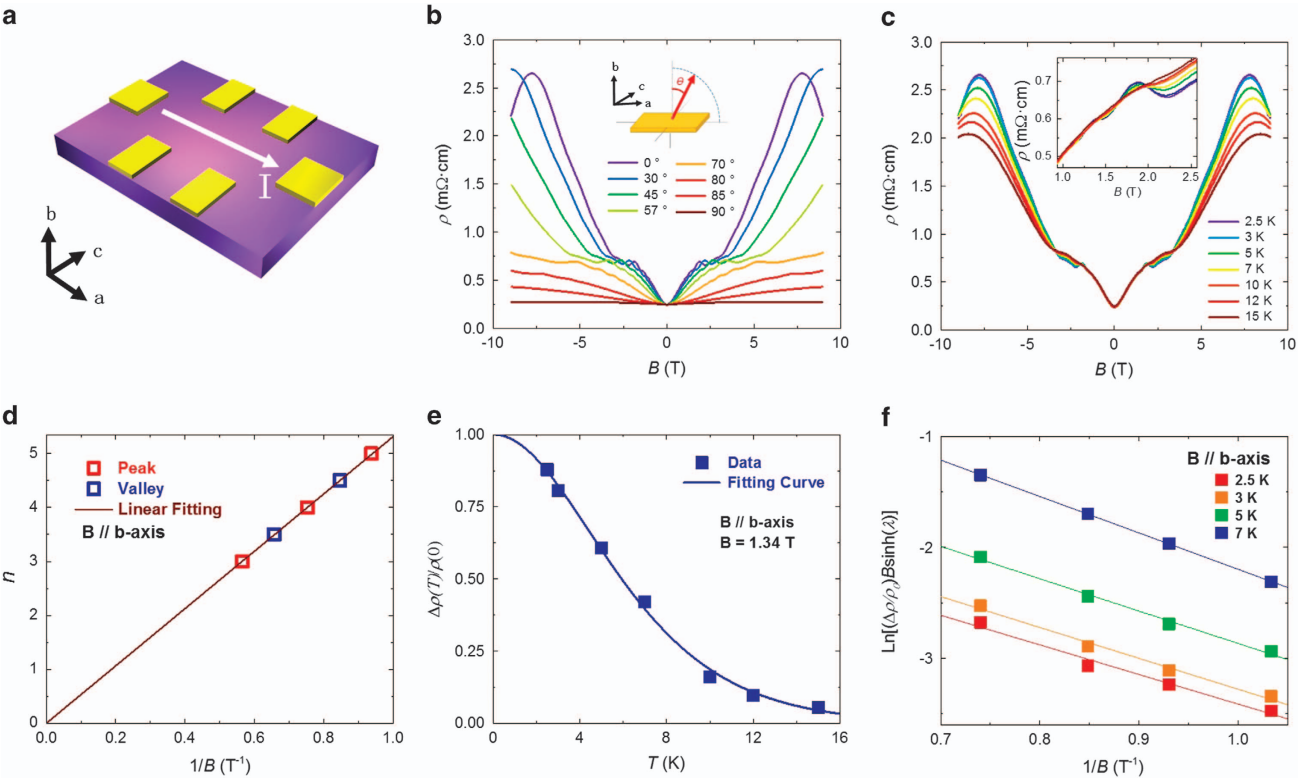

Figure 3 Magneto-transport measurements in $ZrTe_5$. (**a**) Schematic drawing of the transport measurements. A constant current was applied along the a-axis. (**b**) Angle dependence of magnetoresistivity (MR) at 2.5 K. The Shubnikov–de Haas (SdH) oscillations are observed at different angles. (**c**) MR at different temperatures with $\theta = 0°$. The oscillations are not observable above 20 K. The inset is an enlarged view of the oscillations. (**d**) Landau fan diagram at $\theta = 0°$. The nontrivial Berry phase can be clearly seen. (**e**) Temperature dependence of the SdH oscillation amplitude at 1.34 T. (**f**) Dingle plot for the extraction of the scattering time.

The layered structure of $ZrTe_5$ provides an ideal platform for the study of such Dirac states.

To acquire an in-depth understanding of the Dirac quasi-particles, we carried out magneto-transport measurements with rotatable field direction. As schematically illustrated in Figure 3a, conventional six-terminal devices were prepared with a constant current applied along the a-axis of the single crystal. Similar to previous studies,[17,18,31] we observed several unique features of $ZrTe_5$, such as the 'resistivity anomaly' and Hall sign reversal at 150 K (refer to Supplementary Figure S4). The anomaly temperature is related to the Fermi-level position relative to the Dirac point.[32] As determined from the Hall effect (Supplementary Figure S5), $ZrTe_5$ has an *n*-type conductivity at low temperatures. Figure 3b exhibits the magnetoresistivity (MR) of $ZrTe_5$ with the magnetic field tilting from the b-axis to the a-axis. It is evident that the rotation of the magnetic field from perpendicular to parallel to the a–c plane causes a sharp decrease of MR. Apart from the giant anisotropic MR, we observed clear SdH oscillations as a result of Landau quantization. The oscillations can be well resolved from the MR (Figure 3b) even with a magnetic field lower than 1 T, which indicates a high carrier mobility in $ZrTe_5$, consistent with the Hall effect measurements (Supplementary Figures S5 and 6). The amplitude of the oscillations decreases with increasing temperature, but the oscillatory frequency remains the same (Figure 3c).

Generally, under perpendicular magnetic field *B*, closed cyclotron orbits follow the Lifshitz–Onsager quantization rule,

$$S_F \frac{\hbar}{eB} = 2\pi(n+\gamma) = 2\pi\left(n+\frac{1}{2}-\frac{\phi_B}{2\pi}\right) \quad (3)$$

where S_F is the cross-sectional area of the Fermi surface related to the Landau index *n*, and ϕ_B is a geometrical phase known as Berry phase. In a Dirac system, the *k*-space cyclotron orbits enclose a Dirac point so that there exists a 'zero mode' that does not shift with *B*, resulting in a non-trivial Berry phase $\phi_B = \pi$.[14,15,33] Furthermore, γ, defined as $\gamma \equiv 1/2 - \phi_B/2\pi$, can be quantitatively determined by analyzing the intercept of Landau fan diagram from the SdH oscillations. The non-trivial Berry phase generally serves as key evidence for Dirac fermions and has been observed in several well-known Dirac materials such as graphene,[2,14] topological insulator[34,35] and Cd_3As_2.[36,37] Here, we present the Landau fan diagram in Figure 3d, where *n* and $1/B_n$ are extracted from the peak positions in the MR curves. We only use the MR data below 2T in this plot as the SdH oscillations are overwhelmed by a huge shoulder-like MR background at higher fields. By performing a linear fit, the intercept on the y-axis is determined to be 0 ± 0.04, corresponding to the non-trivial Berry phase. If this was a classical narrow bandgap semiconductor, the Berry phase should have become a trivial state with the offset value reaching 0.5. In addition, the slope of the Landau fan diagram gives the frequency of the SdH oscillation, $F = 5.3$T, corresponding to an extremely small Fermi surface of $S_F = 8 \times 10^{-5}$Å^{-2}.

Important transport parameters can be obtained from the SdH oscillation analysis.[38] The temperature dependence of the oscillation amplitude $\Delta\rho$ is shown in Figure 3e that is described by the formula $\Delta\rho(T) = \Delta\rho(0)\lambda(T)/\sinh(\lambda(T))$. The thermal factor $\lambda(T)$ is given by $\lambda(T) = 2\pi^2 k_B T m^*/\hbar eB$, where k_B is the Boltzmann's constant and m^* is the effective mass. By performing the best fit to the equation,

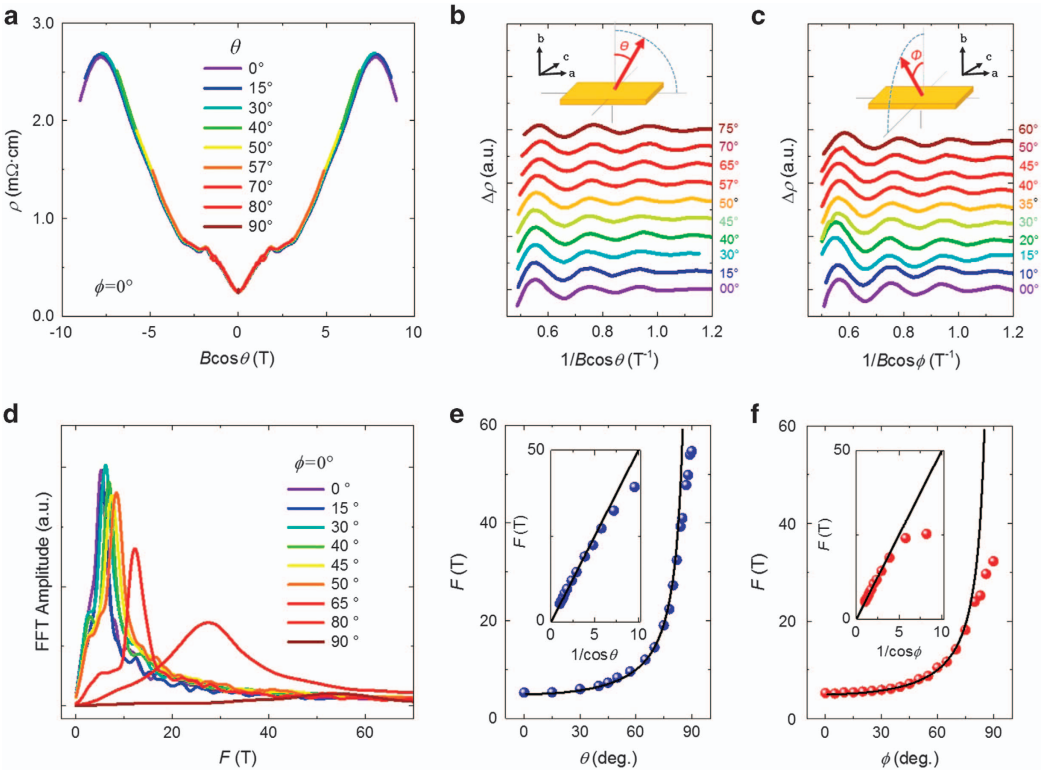

Figure 4 Angle-dependent Magneto-transport measurements in $ZrTe_5$. (**a**) Resistivity versus magnetic field. Data for differentθ, denoted by different colors, overlap with each other, indicating a quasi-two-dimensional (2D) behavior. (**b**, **c**) The oscillatory component $\Delta\rho$ plotted against $1/B$ cos (θ) or $1/B$ cos (ϕ) for B rotation along c-axis and a-axis. (**d**) Fast Fourier transform (FFT) spectra for differentθ. (**e**, **f**) Oscillation frequency plotted with angle. The black curve shows an ideal 2D behavior.

a small effective mass of $m^* = 0.03\ m_e$ is derived, with m_e being the electron mass. Thus, $v_F = 5 \times 10^5$ m s^{-1} can be calculated based on $\hbar k_F = m^* v_F$. Note that the v_F values extracted from the magneto-optics, low-temperature transport and angle-resolved photoemission experiments are of the same order of magnitude but with finite variations, probably because of the electron–phonon interaction[39,40] or extrinsic effect.[41] We can also estimate the quantum lifetime τ by considering the Dingle factor e^{-D}, where $D = 2\pi^2 E_F/\tau e B v_F^2$. Note that $\Delta R/R_0$ is proportional to $(\lambda(T)/\sinh(\lambda(T)))e^{-D}$, and hence the lifetime can be inferred from the slope in the logarithmic plot (Figure 3f). By using $m^* = 0.03\ m_e$, the quantum lifetime of $ZrTe_5$ can be estimated to be $\tau = 1 \times 10^{-12}$ s. A relatively high quantum mobility can be acquired by $\mu = e\tau/m^* = 7 \times 10^4$ cm^2 Vs^{-1}. Our conclusion in a–c plane is consistent with previous reports.[7,25,26]

As we discussed above, one needs to check different crystal orientations to understand the dimensionality of the Dirac fermions. To investigate the overall Fermi surface geometry in $ZrTe_5$, we performed angle-dependent magneto-transport measurements. As shown in Figure 4a, MR with different field directions is distinguished by colors. A noticeable feature is that all curves overlap with each other when plotted against B cos θ. At $\theta = 90°$, the longitudinal MR is almost fully suppressed. The close relationship between the MR ratio and out-of-plane magnetic field indicates a 2D-like behavior of the detected orbit. The shape of the overall Fermi sphere can be mapped by the angle-dependent SdH oscillations. The negative MR is observed that possibly arises from the axial anomaly.[42] The small amplitude of the negative MR could be attributed to the relatively high Fermi level.[42] Figures 4b and c demonstrate the extracted SdH oscillations, while the magnetic field was tilted from the b-axis to the a-axis and from the b-axis to the c-axis. Similar to the MR background, which are overlapped in the scale of B cos θ, the peaks and valleys of the subtracted oscillations are aligned when plotted with respect to B cos θ, in stark contrast with those isotropic 3D systems.[43] Figure 4d shows a fast Fourier transform analysis of the SdH oscillations. The single-peak feature in the fast Fourier transform spectra corresponds to a single-band transport. For an ideal 2D system, the oscillation frequency F increases linearly with 1/cos θ and becomes infinite at $\theta = 90°$ because of the infinite cross-section of Fermi surface. In Figures 4e and f, we plotted the ideal 2D curve following the 1/cos θ rule. Here, the experimental oscillation frequency F increases with 1/cos θ and shows a saturation behavior with small deviations when approaching 90°. The saturation of the frequency suggests a large but not infinite Fermi surface on the b–c plane. Combining the trend of the MR background and the SdH oscillations with various field directions, we can conclude that the Fermi surface in $ZrTe_5$ is highly anisotropic and shows a long rod-like shape in the reciprocal space, thus possessing a quasi-2D behavior in real space. Here, a single-band model is adopted based on the linear Hall effect and single-frequency SdH oscillations at low temperatures (for more detailed discussions, refer to section XII of the Supplementary Information).

We have revealed that the Berry phase extracted from the SdH oscillations in the a–c plane is exactly π, corresponding to a topological nontrivial state. However, the same experiments on other orthogonal axes suggest an unexpected trivial state with the complete elimination of the Berry phase (Supplementary Figure S12). The anomalous features of the Berry phase along different crystal orientations drives

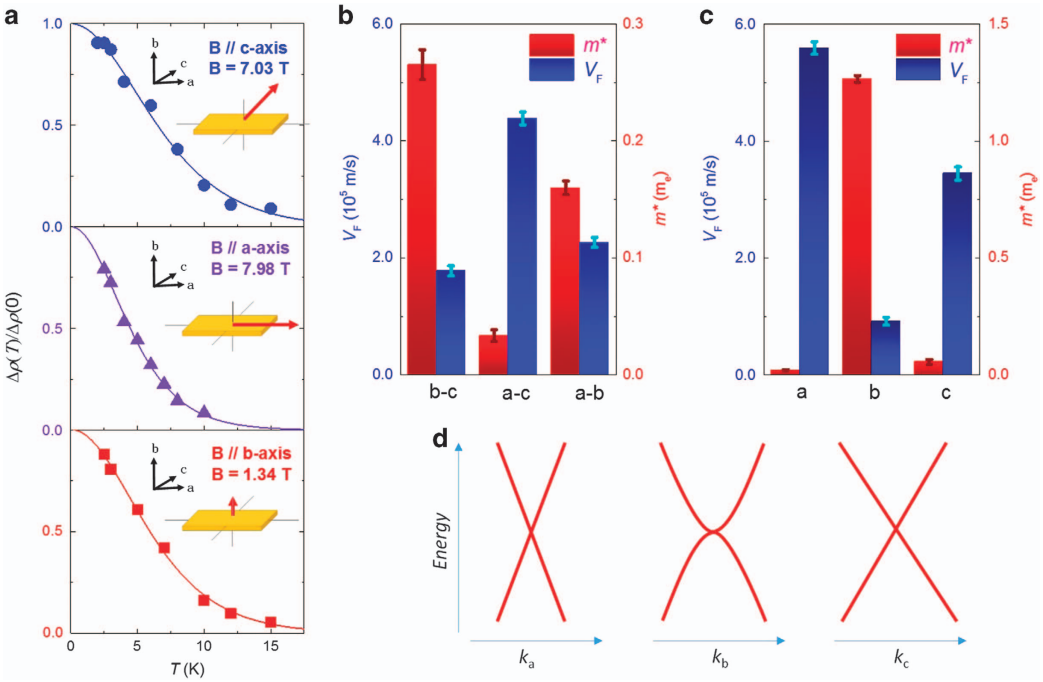

Figure 5 Dispersion characteristics along orthogonal axes. (**a**) The temperature dependence of the Shubnikov–de Haas (SdH) oscillation amplitude for the magnetic field parallel to the c-axis (upper), the a-axis (middle) and the b-axis (lower). (**b**) The effective mass and Fermi velocity retracted from the SdH oscillations in different crystal planes. (**c**) The effective mass and Fermi velocity calculated from (**b**) based on the ellipsoid model. (**d**) A schematic drawing for dispersion characteristics along different orientations. Dirac dispersion is found along the a- and c-axes and nonlinear dispersion along the b-axis. The detail k_b dispersion needs to be investigated using high-resolution angle-resolved photoemission spectroscopy (ARPES) spectroscopy.

us to further analyze the SdH oscillations on all three orthogonal axes for a detailed understanding of band dispersion characteristics. Figure 5a is the oscillation amplitude plotted as a function of temperature. The best fit to those data yields the effective mass for each plane (k_b-k_c, k_a-k_c and k_a-k_b). The Fermi velocity of each plane can also be calculated as discussed above. The a–c plane shows a much smaller m^* and a larger v_F compared with the other two (Figure 5b). This value in the a–c plane (5×10^5 m s^{-1}) is identical to the previous report (5×10^5 m s^{-1})[25] but slightly smaller than those studied by ARPRES (8×10^5 m s^{-1}).[7] As mentioned earlier, the parameters derived from the Landau quantization through transport and magneto-optics are an average value over the closed cyclotron orbit. With the low Fermi level in $ZrTe_5$, the boundary of the Brillouin zone should not have a large impact on the shape of the Fermi surface. Thus, we can safely take the Fermi surface as ellipsoid, and the Fermi velocity (effective mass) of each plane is described as, for example, $v_{a-c}=\sqrt{v_a v_c}$. Here, v_a and v_c are the corresponding Fermi velocity along k_a and k_c, respectively. The transport parameters along the different axes are extracted as shown in Figure 5c. The m^* (red bar) shows a strong anisotropy with a large enhancement along b-axis. It is natural to observe the relatively small effective masses of 0.02 m_e and 0.05 m_e in the a-axis and the c-axis, respectively, consistent with the observation of a massless Dirac fermion in the a–c plane from our magneto-optics experiments. However, the large effective mass of 1.3 m_e along the b-axis is unexpected for the conventional 3D Dirac materials. Note that the crystal is stacked by the layers on the a–c plane along b-axis. The large effective mass may be denoted by the quadratic band dispersion[44] because of the weak interlayer coupling as illustrated in Figure 5d. Thus, we use 'quasi-2D' to describe the Dirac dispersion nature in $ZrTe_5$ that is different from Sr_2RuO_4,[45] or layered organic superconductors[46] whose Fermi surface is in a warped cylindrical shape and stays open along a certain direction in the Brillouin zone. The much lower Fermi velocity (Figure 5c) and quantum mobility (Supplementary Figure S9) along the b-axis also support our assumption. We would like to emphasize that the middle panel in Figure 5d is a schematic drawing to show the non-Dirac dispersion. An ultra-high-resolution APRES measurement along the b-axis direction is required for the detailed dispersion. On the other hand, there is a relatively large difference in both m^* and v_F between the a-axis and the c-axis, revealing an anisotropy in the in-plane dispersion of the Dirac cone. We can use the extracted Fermi velocity along each axis to estimate the overall average Fermi velocity of 6×10^4 m s^{-1} that is an order of magnitude lower than that in the a–c plane. This value also shows a quantitative agreement with previous zero-field infrared spectroscopy experiments (3×10^4 m s^{-1}),[26] where the infrared spectrum without a magnetic field includes information along all three axes, thus providing the overall Fermi velocity. Both the low-temperature transport and infrared spectroscopy measurements[26] suggest an incredibly small Fermi velocity along the b-axis and therefore well justify the quasi-2D nature of $ZrTe_5$.

Importantly, the quasi-2D feature of the massless fermions is further evidenced by transport measurements on a high-mobility sample of 5×10^4 cm^2 Vs^{-1}, as elaborated in Supplementary Information section XIV. The non-trivial Berry phase is not preserved along all the directions in the small magnetic field region that clearly rules out a 3D Dirac semimetal state. Another important evidence is the observation of the bulk QHE plateaus with non-trivial Berry phase in the a–c plane that strongly suggests the presence of the quasi-2D Dirac fermions, as also demonstrated in $EuMnBi_2$.[47]

The *ab initio* calculations have predicted the interlayer binding energy for $ZrTe_5$ to be 12.5 meV $Å^{-1}$, a comparable value to graphite (9.3 meV $Å^{-1}$), suggesting a weak interlayer coupling.[48] Using the conventional Scotch tape method, we have also successfully exfoliated $ZrTe_5$ into 2D thin flakes or 1D nano wires (Supplementary Figure S10). We found that, upon exfoliation, not only is the interplane van der Waals force easy to overcome but also that the in-plane Te zigzag chains are readily broken, thus developing a quasi-1D structure (Supplementary Figure S11). The relatively weak bond along the c-axis may be the reason for the increase of $m^\star$ and the decrease of v_F, similar to the case of the b-axis. We also show that the natural 1D structure can be achieved upon exfoliation that promises related studies such as density wave in $ZrTe_5$ at low dimension.

DISCUSSION

As both the magneto-optics and magneto-transport measurements were performed near liquid helium temperature, our conclusion of a massless Dirac fermion is valid in the low temperature range. However, the resistivity and Hall measurements near 140 K (Supplementary Figure S4) reveal a metal-semiconductor transition (anomaly peak) along with Hall sign reversal (Supplementary Figure S4), indicating a multi-carrier transport and a complex band structure evolving with temperature. However, for higher temperatures, when thermal energy is larger than the energy level separation ($k_BT > \hbar\omega_c$), Landau quantization is no longer accessible, calling for further experimental efforts to elucidate the detailed band structure. Both the previous[10] and recent[49] photoemission experiments report the observation of a gap opening near the anomaly temperature. It indicates that the observed Dirac point is unstable against thermal perturbation. As we discussed in Supplementary Information section X, the Dirac states that we observed are not likely to originate from the surface states. Recently, several surface-sensitive probes were employed to examine the surface/bulk states in $ZrTe_5$.[7,50] Although it was claimed to be gapped with a 2D-like structure in the bulk through a scanning tunneling microscopy technique, another study using the same technique realized a gapped topological insulator on the surface layer.[50,51] Interestingly, an ARPES measurement suggested that the gap opening decreased with temperature reduction, whereas another separate work concluded for massless Dirac fermions at low temperature.[49] The electronic structure was also discussed theoretically. The gapless bulk state was predicted to possibly coexist with the gapped surface state.[32] Importantly, the calculated band structure is highly sensitive to lattice parameters that can be tuned by using different growth methods or under specific growth conditions.[52] $ZrTe_5$ is likely to be close to the band topology transition and, thus, the topology of the band structure is highly sensitive to the chemical composition and the lattice constants. Those theories could explain the controversial arguments surrounding the possible gap. Detailed study on the surface state and clear ARPES experiments along k_b direction are required to comprehensively understand the overall electronic structure.

In the following, we theoretically outline a situation where one can obtain a linear dispersion along two directions and a quadratic one along the third based on the symmetry analysis of Yang and Nagaosa.[53] For a system with both time reversal and inversion symmetry (which is the case for $ZrTe_5$)[52], an accidental band crossing can be described by the Hamiltonian, $H(k_z,k_x=0,\ k_y=0) = d_0 + d(k_z,m)\Gamma$. Here m is a tunable parameter, $\Gamma = \tau_z$ or $\Gamma = \sigma_z\tau_z$, τ_z is the z component of the Pauli matrices describing the orbital pseudospin, whereas σ_z is the z component of the Pauli matrices corresponding to the real spin. A band crossing can be obtained when $d(k_z,m)$ vanishes. If the inversion operator is given by τ_z, then $d(k_z,m)$ is an even function of the crystal momentum k_z. Consequently, to the lowest order in k_z, $d(k_z, m) \approx m + \frac{1}{2}t_z k_z^2$, where t_z is a constant. By choosing $t_z < 0$, a transition from an insulator to a Dirac semimetal is obtained as m changes sign from negative to positive. Crucially, at the critical point where $m = 0$, the band dispersion is quadratic along k_z, whereas it is linear along k_x and k_y (Figure 5d). Therefore, an energy dispersion in a three-dimensional system, which is quadratic along one direction and linear along the other two, is possible in $ZrTe_5$. The system is at a critical point separating an insulating (or topological insulator) and a 3D Dirac semimetal phase. The phase transition is possibly driven by changes in the lattice constants.

Judging from the Landau fan diagram in Figure 3d, the first Landau level can be accessed within 6 T in the magneto-transport experiment, in stark contrast to the representative Dirac semimetal Cd_3As_2 in which the quantum limit requires a magnetic field of at least 43 T or even larger.[54,55] In general, the higher the Fermi level is, the larger field is demanded to access the quantum limit. The calculated Fermi level is 37 meV (refer to Supplementary Information section VII) that is an order of magnitude lower than that in Cd_3As_2 (typically 200–300 meV). Considering the low Fermi level, the thin flakes of $ZrTe_5$ may also be suitable for static electrical gating, and this may add a new degree of freedom to help understand the anomalous transport behavior along the different axes or at high temperatures. Although the Dirac states in graphene can be destroyed in the double layers,[14] it is of great interest to study the Dirac fermions preserved in $ZrTe_5$ bulk state. Meanwhile, it will be of substantial interest to determine whether it will sustain the Dirac fermions in bulk form or transfer into a quantum spin Hall insulator as theory has predicted when approaching the 2D limit. Further experiments in the nanoscale samples or the ultra-quantum limit of $ZrTe_5$ are currently being pursued.

In conclusion, we confirm the existence of Dirac fermions in bulk $ZrTe_5$ by magneto-optics and SdH oscillations. Angle-dependent quantum oscillations reveal a quasi-2D nature of the Dirac fermions, further supported by the bulk QHE and the angle-dependent Berry phase at low fields. Theoretical analysis implies that the system is at the critical point between the Dirac semimetal phase and the topological insulator phase. The unusual interlayer dispersion characteristics, low Fermi level and van der Waals structure demonstrate $ZrTe_5$ as an intriguing system for both the fundamental studies and device applications.

CONFLICT OF INTEREST

The authors declare no competing financial interests.

ACKNOWLEDGEMENTS

This work was supported by the National Young 1000 Talent Plan, the Program for Professors of Special Appointment (Eastern Scholar) at Shanghai Institutions of Higher Learning, the National Natural Science Foundation of China (61322407 and 11474058) and the Chinese National Science Fund for Talent Training in Basic Science (J1103204). Part of the sample fabrication was performed at Fudan Nano-fabrication Laboratory. A portion of this work was performed at the National High Magnetic Field Laboratory that is supported by National Science Foundation Cooperative Agreement No. DMR-1157490 and the State of Florida.

Author contributions: FX conceived the idea and supervised the experiments. XY and CZ carried out the growth, magneto-transport measurements and data analysis. XY and CZ performed the magneto-optics experiments. YL, SS, XS and JZ helped with the growth. YL, CS, and HY helped with the data analysis. AN and SS performed the band structure modeling. JX, HY and ZA

assisted in the infrared property characterizations. XY, CZ and FX wrote the paper with help from all the other authors.

1 Novoselov, K., Geim, A. K., Morozov, S., Jiang, D., Katsnelson, M., Grigorieva, I., Dubonos, S. & Firsov, A. Two-dimensional gas of massless Dirac fermions in graphene. *Nature* **438**, 197–200 (2005).
2 Zhang, Y., Tan, Y. W., Stormer, H. L. & Kim, P. Experimental observation of the quantum Hall effect and Berry's phase in graphene. *Nature* **438**, 201–204 (2005).
3 Fiori, G., Bonaccorso, F., Iannaccone, G., Palacios, T., Neumaier, D., Seabaugh, A., Banerjee, S. K. & Colombo, L. Electronics based on two-dimensional materials. *Nat. Nanotechnol.* **9**, 768–779 (2014).
4 Wang, Q. H., Kalantar-Zadeh, K., Kis, A., Coleman, J. N. & Strano, M. S. Electronics and optoelectronics of two-dimensional transition metal dichalcogenides. *Nat. Nanotechnol.* **7**, 699–712 (2012).
5 Kim, J., Baik, S. S., Ryu, S. H., Sohn, Y., Park, S., Park, B.-G., Denlinger, J., Yi, Y., Choi, H. J. & Kim, K. S. Observation of tunable band gap and anisotropic Dirac semimetal state in black phosphorus. *Science* **349**, 723–726 (2015).
6 Qian, X., Liu, J., Fu, L. & Li, J. Quantum spin Hall effect in two-dimensional transition metal dichalcogenides. *Science* **346**, 1344–1347 (2014).
7 Li, Q., Kharzeev, D. E., Zhang, C., Huang, Y., Pletikosic, I., Fedorov, A. V., Zhong, R. D., Schneeloch, J. A., Gu, G. D. & Valla, T. Chiral magnetic effect in $ZrTe_5$. *Nat Phys* **12**, 550–554 (2016).
8 Chen, R. Y., Zhang, S. J., Schneeloch, J. A., Zhang, C., Li, Q., Gu, G. D. & Wang, N. L. Optical spectroscopy study of the three-dimensional Dirac semimetal $ZrTe_5$. *Phys. Rev. B* **92**, 075107 (2015).
9 Chen, R. Y., Chen, Z. G., Song, X. Y., Schneeloch, J. A., Gu, G. D., Wang, F. & Wang, N. L. Magnetoinfrared spectroscopy of Landau levels and Zeeman splitting of three-dimensional massless Dirac fermions in $ZrTe_5$. *Phys. Rev. Lett.* **115**, 176404 (2015).
10 McIlroy, D. N., Moore, S., Zhang, D., Wharton, J., Kempton, B., Littleton, R., Wilson, M., Tritt, T. M. & Olson, C. G. Observation of a semimetal–semiconductor phase transition in the intermetallic $ZrTe_5$. *J. Phys. Condens. Matter* **16**, L359–L365 (2004).
11 Xu, X., Yao, W., Xiao, D. & Heinz, T. F. Spin and pseudospins in layered transition metal dichalcogenides. *Nat. Phys.* **10**, 343–350 (2014).
12 Geim, A. K. & Grigorieva, I. V. Van der Waals heterostructures. *Nature* **499**, 419–425 (2013).
13 Xu, M., Liang, T., Shi, M. & Chen, H. Graphene-like two-dimensional materials. *Chem. Rev.* **113**, 3766–3798 (2013).
14 Neto, A. C., Guinea, F., Peres, N., Novoselov, K. S. & Geim, A. K. The electronic properties of graphene. *Rev. Mod. Phys.* **81**, 109 (2009).
15 Basov, D. N., Fogler, M. M., Lanzara, A., Wang, F. & Zhang, Y. *Colloquium*: graphene spectroscopy. *Rev. Mod. Phys.* **86**, 959–994 (2014).
16 Young, A. F. & Kim, P. Quantum interference and Klein tunnelling in graphene heterojunctions. *Nat. Phys.* **5**, 222–226 (2009).
17 Skelton, E., Wieting, T., Wolf, S., Fuller, W., Gubser, D. U., Francavilla, T. & Levy, F. Giant resistivity and X-ray diffraction anomalies in low-dimensional $ZrTe_5$ and $HfTe_5$. *Solid State Commun.* **42**, 1–3 (1982).
18 Fuller, W., Wolf, S., Wieting, T., LaCoe, R., Chaikin, P. & Huang, C. Pressure effects in $HfTe_5$ and $ZrTe_5$. *J. Phys. Colloq.* **44**, C3-1709-C1703–1712 (1983).
19 Kamm, G., Gillespie, D., Ehrlich, A., Wieting, T. & Levy, F. Fermi surface, effective masses, and Dingle temperatures of $ZrTe_5$ as derived from the Shubnikov–de Haas effect. *Phys. Rev. B* **31**, 7617 (1985).
20 Jones, T., Fuller, W., Wieting, T. & Levy, F. Thermoelectric power of $HfTe_5$ and $ZrTe_5$. *Solid State Commun.* **42**, 793–798 (1982).
21 Littleton, R. IV, Tritt, T. M., Kolis, J. & Ketchum, D. Transition-metal pentatellurides as potential low-temperature thermoelectric refrigeration materials. *Phys. Rev. B* **60**, 13453 (1999).
22 Whangbo, M.-H., DiSalvo, F. & Fleming, R. Electronic structure of $ZrTe_5$. *Phys. Rev. B* **26**, 687 (1982).
23 Vafek, O. & Vishwanath, A. Dirac fermions in solids: from high-Tc cuprates and graphene to topological insulators and weyl semimetals. *Annu. Rev. Condens. Matter Phys.* **5**, 83–112 (2014).
24 Assaf, B., Phuphachong, T., Volobuev, V., Inhofer, A., Bauer, G., Springholz, G., de Vaulchier, L. & Guldner, Y. Massive and massless Dirac fermions in Pb(1-x)Sn(x)Te topological crystalline insulator probed by magneto-optical absorption. *Sci. Rep.* **6**, 20323 (2016).
25 Chen, R., Chen, Z., Song, X.-Y., Schneeloch, J., Gu, G., Wang, F. & Wang, N. Magnetoinfrared spectroscopy of Landau levels and Zeeman splitting of three-dimensional massless Dirac fermions in $ZrTe_5$. *Phys. Rev. Lett.* **115**, 176404 (2015).
26 Chen, R., Zhang, S., Schneeloch, J., Zhang, C., Li, Q., Gu, G. & Wang, N. Optical spectroscopy study of the three-dimensional Dirac semimetal $ZrTe_5$. *Phys. Rev. B* **92**, 075107 (2015).
27 Orlita, M., Basko, D. M., Zholudev, M. S., Teppe, F., Knap, W., Gavrilenko, V. I., Mikhailov, N. N., Dvoretskii, S. A., Neugebauer, P., Faugeras, C., Barra, A. L., Martinez, G. & Potemski, M. Observation of three-dimensional massless Kane fermions in a zinc-blende crystal. *Nat. Phys.* **10**, 233–238 (2014).
28 Jiang, Z., Henriksen, E., Tung, L., Wang, Y.-J., Schwartz, M., Han, M., Kim, P. & Stormer, H. Infrared spectroscopy of Landau levels of graphene. *Phys. Rev. Lett.* **98**, 197403 (2007).
29 Liu, Z., Zhou, B., Zhang, Y., Wang, Z., Weng, H., Prabhakaran, D., Mo, S.-K., Shen, Z., Fang, Z. & Dai, X. Discovery of a three-dimensional topological Dirac semimetal, Na_3Bi. *Science* **343**, 864–867 (2014).
30 Liu, Z. K., Jiang, J., Zhou, B., Wang, Z. J., Zhang, Y., Weng, H. M., Prabhakaran, D., Mo, S. K., Peng, H., Dudin, P., Kim, T., Hoesch, M., Fang, Z., Dai, X., Shen, Z. X., Feng, D. L., Hussain, Z. & Chen, Y. L. A stable three-dimensional topological Dirac semimetal Cd_3As_2. *Nat. Mater.* **13**, 677–681 (2014).
31 Tritt, T. M., Lowhorn, N. D., Littleton, R. IV, Pope, A., Feger, C. & Kolis, J. Large enhancement of the resistive anomaly in the pentatelluride materials $HfTe_5$ and $ZrTe_5$ with applied magnetic field. *Phys. Rev. B* **60**, 7816 (1999).
32 Pariari, A. & Mandal, P. Coexistence of topological Dirac fermions in the surface and three-dimensional Dirac cone state in the bulk of $ZrTe_5$ single crystal *arXiv preprint arXiv:160305175* (2016).
33 Hasan, M. Z. & Kane, C. L. Colloquium: topological insulators. *Rev. Mod. Phys.* **82**, 3045–3067 (2010).
34 Analytis, J. G., McDonald, R. D., Riggs, S. C., Chu, J.-H., Boebinger, G. & Fisher, I. R. Two-dimensional surface state in the quantum limit of a topological insulator. *Nat. Phys.* **6**, 960–964 (2010).
35 Zhang, C., Yuan, X., Wang, K., Chen, Z. G., Cao, B., Wang, W., Liu, Y., Zou, J. & Xiu, F. Observations of a metal–insulator transition and strong surface states in $Bi_{2-x}Sb_xSe_3$ thin films. *Adv. Mater* **26**, 7110–7115 (2014).
36 He, L. P., Hong, X. C., Dong, J. K., Pan, J., Zhang, Z., Zhang, J. & Li, S. Y. Quantum transport evidence for the three-dimensional Dirac semimetal phase in Cd_3As_2. *Phys. Rev. Lett.* **113**, 246402 (2014).
37 Cao, J., Liang, S., Zhang, C., Liu, Y., Huang, J., Jin, Z., Chen, Z. G., Wang, Z., Wang, Q., Zhao, J., Li, S., Dai, X., Zou, J., Xia, Z., Li, L. & Xiu, F. Landau level splitting in Cd_3As_2 under high magnetic fields. *Nat. Commun.* **6**, 7779 (2015).
38 Xiu, F., He, L., Wang, Y., Cheng, L., Chang, L. T., Lang, M., Huang, G., Kou, X., Zhou, Y., Jiang, X., Chen, Z., Zou, J., Shailos, A. & Wang, K. L. Manipulating surface states in topological insulator nanoribbons. *Nat. Nanotechnol.* **6**, 216–221 (2011).
39 Park, C.-H., Giustino, F., Cohen, M. L. & Louie, S. G. Velocity renormalization and carrier lifetime in graphene from the electron-phonon interaction. *Phys. Rev. Lett.* **99**, 086804 (2007).
40 Siegel, D. A., Park, C.-H., Hwang, C., Deslippe, J., Fedorov, A. V., Louie, S. G. & Lanzara, A. Many-body interactions in quasi-freestanding graphene. *Proc. Natl Acad. Sci. USA* **108**, 11365–11369 (2011).
41 Wolos, A., Szyszko, S., Drabinska, A., Kaminska, M., Strzelecka, S. G., Hruban, A., Materna, A. & Piersa, M. Landau-level spectroscopy of relativistic fermions with low fermi velocity in the Bi_2Te_3 three-dimensional topological insulator. *Phys. Rev. Lett.* **109**, 247604 (2012).
42 Goswami, P., Pixley, J. H. & Das Sarma, S. Axial anomaly and longitudinal magnetoresistance of a generic three-dimensional metal. *Phys. Rev. B* **92**, 075205 (2015).
43 Liang, T., Gibson, Q., Ali, M. N., Liu, M., Cava, R. J. & Ong, N. P. Ultrahigh mobility and giant magnetoresistance in the Dirac semimetal Cd3As2. *Nat. Mater.* **14**, 280–284 (2014).
44 Park, J., Lee, G., Wolff-Fabris, F., Koh, Y., Eom, M., Kim, Y., Farhan, M., Jo, Y., Kim, C. & Shim, J. Anisotropic Dirac fermions in a Bi square net of $SrMnBi_2$. *Phys. Rev. Lett.* **107**, 126402 (2011).
45 Mackenzie, A. P. & Maeno, Y. The superconductivity of Sr_2RuO_4 and the physics of spin-triplet pairing. *Rev. Mod. Phys.* **75**, 657 (2003).
46 Singleton, J., Goddard, P. A., Ardavan, A., Coldea, A. I., Blundell, S. J., McDonald, R. D., Tozer, S. & Schlueter, J. A. Persistence to high temperatures of interlayer coherence in an organic superconductor. *Phys. Rev. Lett.* **99**, 027004 (2007).
47 Masuda, H., Sakai, H., Tokunaga, M., Yamasaki, Y., Miyake, A., Shiogai, J., Nakamura, S., Awaji, S., Tsukazaki, A. & Nakao, H. Quantum Hall effect in a bulk antiferromagnet $EuMnBi_2$ with magnetically confined two-dimensional Dirac fermions. *Sci. Adv.* **2**, e1501117 (2016).
48 Weng, H., Dai, X. & Fang, Z. Transition-metal pentatelluride $ZrTe_5$ and $HfTe_5$: a paradigm for large-gap quantum spin hall insulators. *Phys. Rev. X* **4**, 011002 (2014).
49 Zhang, Y., Wang, C., Yu, L., Liu, G., Liang, A., Huang, J., Nie, S., Zhang, Y., Shen, B. & Liu, J. Electronic evidence of temperature-induced Lifshitz transition and topological nature in $ZrTe_5$ *arXiv preprint arXiv:160203576* (2016).
50 Li, X.-B., Huang, W.-K., Lv, Y.-Y., Zhang, K.-W., Yang, C.-L., Zhang, B.-B., Chen, Y., Yao, S.-H., Zhou, J. & Lu, M.-H. Robust topological edge states at the perfect surface step edge of topological insulator $ZrTe_5$ *arXiv preprint arXiv:160105930* (2016).
51 Wu, R., Ma, J.-Z., Zhao, L.-X., Nie, S.-M., Huang, X., Yin, J.-X., Fu, B.-B., Richard, P., Chen, G.-F. & Fang, Z. Experimental evidence of large-gap two-dimensional topological insulator on the surface of $ZrTe_5$ *arXiv preprint arXiv:160107056* (2016).
52 Weng, H., Dai, X. & Fang, Z. Transition-metal pentatelluride $ZrTe_5$ and $HfTe_5$: a paradigm for large-gap quantum spin hall insulators. *Phys. Rev. X* **4**, 011002 (2014).
53 Yang, B.-J. & Nagaosa, N. Classification of stable three-dimensional Dirac semimetals with nontrivial topology. *Nat. Commun.* **5**, 4898 (2014).
54 Zhao, Y., Liu, H., Zhang, C., Wang, H., Wang, J., Lin, Z., Xing, Y., Lu, H., Liu, J., Wang, Y., Brombosz, S. M., Xiao, Z., Jia, S., Xie, X. C. & Wang, J. Anisotropic fermi surface and quantum limit transport in high mobility three-dimensional Dirac semimetal Cd_3As_2. *Phys. Rev. X* **5**, 031037 (2015).
55 Cao, J., Liang, S., Zhang, C., Liu, Y., Huang, J., Jin, Z., Chen, Z.-G., Wang, Z., Wang, Q., Zhao, J., Li, S., Dai, X., Zou, J., Xia, Z., Li, L. & Xiu, F. Landau level splitting in Cd_3As_2 under high magnetic fields. *Nat. Commun.* **6**, 7779 (2015).

Supplementary Information accompanies the paper on the NPG Asia Materials website (http://www.nature.com/am)